Controlling chaos in higher dimensional maps with constant feedback: An analytical approach

Cristian Wieland*

(Received 20 November 2001; published 12 July 2002)

We introduce two methods to control chaos in higher-dimensional discrete maps with constant feedback. It is analytically shown for a general class of function vectors that chaotic attractors can be converted into fixed point attractors. Additionally, a method to choose an appropriate constant feedback is presented. The application of these methods does not require *a priori* knowledge of system equations, since time series information can be used. Desired periodic orbits can be accessed by varying the constant feedback. As an example, the methods are applied to the Hénon map.

DOI: 10.1103/PhysRevE.66.016205 PACS number(s): 05.45.Gg

I. INTRODUCTION

After the detection of chaos, the current opinion of scientists was that chaotic motion was neither predictable nor controllable because of the sensitive dependence on initial conditions of chaotic systems, e.g., see Ref. [1]. Perturbations in the system's behavior for the purpose of control would only generate different chaotic behavior. This was a fallacy, as the pioneering work of Ott, Grebogi, and Yorke (OGY-method) in 1990 showed. Since then the problem of controlling chaos has been an attractive field of research, especially among physicists over the past decade, yielding two ways to control chaos. The first way is to stabilize unstable periodic orbits embedded within a chaotic attractor represented, for example, by the well-known OGY method [2] that applies small perturbations, determined by closed-loop control techniques, to an accessible system parameter and by Pyragas' delayed feedback control (DFC) [3], where continuous linear feedback is added to the system at each computational time step. The second way, called suppressing chaos, is to convert chaotic system behavior into desired periodic behavior. Some well-known methods are, for example, adaptive control algorithms such as [4,5], the use of noise [6,7], and the constant feedback method (CF) [8], which will be investigated in detail in this work. Although a great number of publications on controlling chaos exist, many approaches suffer from a lack of precise analytical description, i.e., the applicability of methods is only verified numerically or in an experimental environment; note that numerical evidence or experiments cannot assure periodicity or convergence in general. In Ref. [9] examples are listed. This procedure has the disadvantage that a transfer of chaos control methods from certain numerical examples to other more practical cases is likely to fail. A precise analytical description, although in many cases hard to meet, is thus advisable and will be followed when we introduce methods for controlling chaos.

Section II commences with an overview of previous work on CF. There it will be shown that publications on CF either concentrated on a special kind of one-dimensional discrete map with unimodal system function or are restricted to numerical results in the higher-dimensional case. Hence, there exists a lack of theory of controlling chaos in higher-dimensional discrete maps with CF. The question to be dealt with is thus whether there is a way to control chaos in n-dimensional discrete maps by simply adding a constant feedback. For this, the original CF and a modified constant feedback method (MCF) are investigated in Sec. III. It will be proven analytically, and not only by numerical results, that both methods are suitable for controlling chaos in higher-dimensional discrete systems. Furthermore, a method for choosing an appropriate control parameter is also provided. In Sec. IV, some numerical results are presented. In addition it will be shown that possible new fixed points as well as the constant feedback vector can be determined from time series information. This paper closes with a conclusion in which the results for CF and MCF are summarized and compared to other methods.

II. PREVIOUS WORK

Parthasarathy and Sinha [8] presented a simple method called constant feedback to control chaotic oscillations in one-dimensional discrete maps of the form

$$x_{t+1}=f(x_t), \tag{2.1}$$

where $f:I\rightarrow I$ is a $\boldsymbol{C}^2$ unimodal function on the interval $I\subseteq[0,\infty)$. A constant feedback k with $k\in\mathbb{R}$ is added at each iteration to the right-hand side of Eq. (2.1) and it follows that

$$x_{t+1}=f(x_t)+k. \tag{2.2}$$

Parthasarathy and Sinha applied CF to the logistic, the exponential map for specific choice of parameters and initial conditions, and observed convergence to fixed points and periodic points. Gueron was the first to present an analytical description of CF [9], as he proved that a certain k exists, such that the system in Eq. (2.1) converges to a fixed point if f is a unimodal function on $\mathbb{R}^+$.

An extension of CF to higher-dimensional maps is suitable for controlling spatiotemporal chaos in coupled map lattices [10]. Parekh *et al.* added a constant feedback $k(i)$ to each lattice site i with $i=1,\ldots,n$ to stabilize n-dimensional systems in any desired periodic state. They gave a numerical

*Present address: Department of Economics, University of Osnabrueck, 49069 Osnabrueck, Germany; electronic address: cwieland@oec.uni-osnabrueck.de

example, in which f denotes the logistic map, and remarked that in general f has to be a unimodal function, as in Eq. (2.1).

Parek and Shinha elaborated experimental results by simulating neuronal activities that have to be controlled [11]. Furthermore, they observed chaos suppression with CF in coupled Hénon maps and in a coupled continuous Lorenz system. Osipov *et al.* demonstrated that CF can be used to stabilize chaos in continuous time systems by adding an impulsive function for the Duffing oscillator [12]. Further experimental studies exist in which alteration in dynamics is affected by perturbing a system variable: Corron *et al.* presented two experiments where control is activated if certain variables exceed a threshold [13], which was theoretically reinterpreted for maps in [14]; Korpimäki and Norrdahl observed in an outdoor experiment that reduction of all main predators stabilized the former cyclic behavior of a small rodent population [15]; Hudson *et al.* gained similar results in an experiment with grouse and its parasites [16].

Nevertheless, numerical evidence or experiments cannot assure periodicity or convergence in general. With the exception of the results in Ref. [9] for one-dimensional discrete maps with unimodal functions, neither rigorous conclusions about a general class of nonlinear function nor how to choose an appropriate constant feedback can be found in related literature. It is therefore necessary to deliver a proof that chaos control in n-dimensional maps is achievable when constant feedback is applied. It follows that a systematic method to choose a constant feedback is included and that a general class of functions can be determined. This will be done for CF and MCF in the following sections.

III. ANALYTICAL RESULTS FOR CF AND MCF

Both feedback methods, CF and MCF, are introduced in the following by considering an n-dimensional map

$$\mathbf{x}_{t+1}=\mathbf{f}(\mathbf{x}_t,\mathbf{p}), \tag{3.1}$$

where $\mathbf{x}_t \in I$ denotes the vector of variables to be studied and $\mathbf{p}\in J\subset\mathbb{R}^r$ is a parameter vector, and $\mathbf{f}:I\to I$, $\boldsymbol{C}^r$, $r\geqslant 1$ with $I\subset\mathbb{R}^n$ is a nonlinear function vector. It is assumed that the map may produce chaotic or cyclic behavior that has to be controlled.

Before CF and MCF are introduced, recall the next theorem for stability of fixed points.

Theorem III.1. A fixed point $\mathbf{x}_*$ of a map $\mathbf{f}$ is asymptotically stable if all eigenvalues of the Jacobian $\mathbf{J}$ at $\mathbf{x}_*$ have moduli less than one.

Proof. See Ref. [17]. □

A lemma is needed to clarify where fixed points occur in discrete maps from a geometrical point of view, i.e., where to find a fixed point on the graph of $\boldsymbol{f}$. Obviously, for $n=1$ fixed points can only be found at intersections of the graph of the system function and the 45° line. This happens if

$$f(x)=g(x) \tag{3.2}$$

with $g(x)=x$. This holds even in higher dimensions, as is shown in the following lemma.

Lemma III.1 Consider a map $\boldsymbol{f}$ and let $\boldsymbol{g}(\boldsymbol{x})=\boldsymbol{x}$ with $\boldsymbol{x}'=[x(1),\ldots,x(n)]$, $\boldsymbol{x}\in\mathbb{R}^n$, then the intersection

$$\boldsymbol{f}(\boldsymbol{x})=\boldsymbol{g}(\boldsymbol{x}) \tag{3.3}$$

is a fixed point.

Proof. A fixed point is defined as $\boldsymbol{x}_*=\boldsymbol{f}(\boldsymbol{x}_*)$ and thus for any $\boldsymbol{x}_*$ it follows that $\boldsymbol{x}_*=\boldsymbol{g}(\boldsymbol{x}_*)$. □

Lemma III is needed to distinguish between the dynamics of a map by iteration and the rule $\boldsymbol{f}$ of a map. The reason for this is that the basic idea of CF and MCF is to shift the graph of $\boldsymbol{f}$ such that $\boldsymbol{g}$ intersects $\boldsymbol{f}$ at any point $\boldsymbol{z}$, bearing in mind that $\boldsymbol{z}$ possesses the stability condition from Theorem III. This is formalized in the following.

A. CF

Applying CF means that the constant feedback vector $\boldsymbol{k}\in\mathbb{R}^n$ is added to the map at each discrete time step t. Or, in other words, we add a constant feedback to each element of the function vector to achieve a shift of the graph of a function vector. For example, the graph of a one-dimensional map is shifted up or down the y axis if CF is applied.

Theorem III.2. Consider a map with $\boldsymbol{f}:I\to I$, $\boldsymbol{C}^r$, $r\geqslant 1$ and $I\subset\mathbb{R}^n$, $\boldsymbol{x}_t\in\mathbb{R}^n$. Let $\boldsymbol{z}\in\mathbb{R}^n$ be a point with $|\lambda_i|<1\ \forall\ i$, where λ_i denotes the ith eigenvalue of the Jacobian of $\boldsymbol{f}$ at $\boldsymbol{z}$. Then there exists a constant feedback vector $\boldsymbol{k}\in\mathbb{R}^n$ with

$$\boldsymbol{k}=\boldsymbol{z}-\boldsymbol{f}(\boldsymbol{z}) \tag{3.4}$$

such that

$$\boldsymbol{x}_{t+1}=\boldsymbol{f}(\boldsymbol{x}_t,\boldsymbol{p})+\boldsymbol{k} \tag{3.5}$$

possesses a stable fixed point at $\boldsymbol{x}_*=\boldsymbol{z}$.

Proof. Eq. (3.5) possesses a fixed point at $\boldsymbol{x}_*=\boldsymbol{z}$ if $\boldsymbol{f}(\boldsymbol{z})+\boldsymbol{k}=\boldsymbol{g}(\boldsymbol{z})$. Inserting Eq. (3.4) gives $\boldsymbol{z}=\boldsymbol{g}(\boldsymbol{z})$. Thus, $\boldsymbol{x}_*=\boldsymbol{z}$ is an asymptotically stable fixed point because of Lemma III.1 and Theorem III.1. □

Note that shifting the graph yields a different basin of attraction. Since the class of function vectors is not further specified, it is difficult to give a general statement on the new basin. Further conditions have to be set up to achieve at least a subset of the new basin of attraction. This is done in the following proposition.

Proposition III.3. Let $\boldsymbol{z}$ lie in a compact set $B\subset\mathbb{R}^n$. Let any other point $\boldsymbol{x}\in B$ have $\max|\lambda|<1$ and $\boldsymbol{x}\neq\boldsymbol{f}(\boldsymbol{x})+\boldsymbol{k}$, then B is at least a subset of the basin of attraction for the fixed point $\boldsymbol{x}_*=\boldsymbol{z}$ of the map in Eq. (3.5).

Proof. The fixed point $\boldsymbol{x}_*=\boldsymbol{z}$ has only stable manifolds described by B because every $\boldsymbol{x}\in B$ has $max|\lambda|<1$. Hence, the map in Eq. (3.5) converges to $\boldsymbol{x}_*=\boldsymbol{z}$ for every $\boldsymbol{x}_0\in B$. □

It is rather more difficult to derive an approach delivering stable higher periodic orbits. Let us consider, for example, a period two cycle of a one-dimensional map. Recall that maps in general have a period two cycle if $x_p=f(f(x_p))$. Thus, we are looking for intersections between the graph of $f(f(x))$ and the 45° line $g(x)=x$. The cycle is stable if all periodic

points have eigenvalues with a modulus smaller than one. By applying CF to a one-dimensional map a period two cycle is obtained if

$$x_p = f(f(x_p)+k)+k, \tag{3.6}$$

since k is added at each iteration. Consequently, the application of CF does not merely shift the graph of $f(f(x))$, but changes the course and, as a consequence, the eigenvalues of points. Thus, Theorem III.2 is inessential in the case of stabilizing higher periodic orbits. Furthermore, the original function vector cannot be used to determine periodic points possessing the stability condition. But, by interpreting Eq. (3.6) as a new map, stability analysis of fixed points is applicable for further studies.

B. MCF

Two possible interpretations of MCF are offered. The first is to assume that the variable vector $\boldsymbol{x}_t$ can be superimposed at each iteration by a constant feedback vector $\boldsymbol{k} \in \mathbb{R}^n$. The second is that after each iteration $\boldsymbol{x}_t + \boldsymbol{k}$ is computed and the following control scheme results:

$$\ldots \boldsymbol{f}(\boldsymbol{x}_{t-1}+\boldsymbol{k}) = \boldsymbol{x}_t \rightarrow \boldsymbol{x}_t + \boldsymbol{k} \rightarrow \boldsymbol{f}(\boldsymbol{x}_t+\boldsymbol{k}) = \boldsymbol{x}_{t+1} \ldots .$$

Thus, applying MCF causes, for example, the graph of a one-dimensional map to be shifted along the x axis. The previous statements lead to the next theorem.

Theorem III.4. Consider a map with $\boldsymbol{f}: I \rightarrow I$, $\boldsymbol{C}^r$, $r \geqslant 1$ and $I \subset \mathbb{R}^n$, $\boldsymbol{x}_t \in \mathbb{R}^n$. Let $\boldsymbol{z} \in \mathbb{R}^n$ be a point with $|\lambda_i| < 1 \ \forall \ i$, where λ_i denotes the ith eigenvalue of the Jacobian of $\boldsymbol{f}$ at $\boldsymbol{z}$. Then there exists a constant feedback vector $\boldsymbol{k} \in \mathbb{R}^n$ with

$$\boldsymbol{k} = \boldsymbol{z} - \boldsymbol{f}(\boldsymbol{z}) \tag{3.7}$$

such that

$$\boldsymbol{x}_{t+1} = f(\boldsymbol{x}_t + \boldsymbol{k}, \boldsymbol{p}) \tag{3.8}$$

possesses a stable fixed point at $\boldsymbol{x}_* = \boldsymbol{z} - \boldsymbol{k}$.

Proof. Let $\tilde{\boldsymbol{f}}(\boldsymbol{x}) = \boldsymbol{f}(\boldsymbol{x}+\boldsymbol{k})$. Then $\boldsymbol{x}_{t+1} = \tilde{\boldsymbol{f}}(\boldsymbol{x})$ possesses a fixed point if $\boldsymbol{z} - \boldsymbol{k} = \tilde{\boldsymbol{f}}(\boldsymbol{z}-\boldsymbol{k})$ and it follows that $\boldsymbol{z} - \boldsymbol{k} = \boldsymbol{f}(\boldsymbol{z})$. Thus, if $\boldsymbol{k} = \boldsymbol{z} - \boldsymbol{f}(\boldsymbol{z})$ then $\boldsymbol{x}_* = \boldsymbol{z} - \boldsymbol{k}$ is an asymptotically stable fixed point of Eq. (3.8) because of Lemma III.1 and Theorem III.1. □

Since the graph is shifted, as in the case of CF, a new basin of attraction is obtained. Further specifications of the function vector lead to the following proposition.

Proposition III.5 Let $\boldsymbol{z}$ lie in a compact set $B \subset \mathbb{R}^n$. Let any other point $\boldsymbol{x} \in B$ have $max|\lambda| < 1$ with $\boldsymbol{x} \neq \boldsymbol{f}(\boldsymbol{x}+\boldsymbol{k})$. Then $B_{-\boldsymbol{k}} = \{\boldsymbol{y} \in \mathbb{R}^n | \boldsymbol{x} \in B, \boldsymbol{y} = \boldsymbol{x} - \boldsymbol{k}\}$ is at least a subset of the basin of attraction for the fixed point $\boldsymbol{x}_* = \boldsymbol{z} - \boldsymbol{k}$ of the map in Eq. (3.8).

Proof. Analogous to Proposition III.5 for CF, with the difference that B is shifted by $\boldsymbol{k}$. □

The same causal relation as in the case of CF makes Theorem III.4 inessential to deliver an appropriate choice for $\boldsymbol{k}$ and, consequently, to stabilize higher periodic orbits. Since the graph of the function vector is changed we have to rely on the reinterpretation of the subjected map as a new map.

IV. NUMERICAL RESULTS

Recall that the aim of the preceding section was to prove convergence of maps with a general class of function vector if these maps are subjected to CF or MCF. The indeed very general outcomes prove general applicability for a huge variety of maps. But, since the graph of the function vector is shifted, it should be clear that a different basin of attraction for the new fixed point is obtained if CF or MCF is applied. Unfortunately, the basin of attraction remains unknown, without further restrictions regarding the function vector. As a matter of fact, it is thus impossible to estimate the robustness of CF and MCF against noise in general. We can only state that if the basin of attraction is a very small area, both methods are more likely to be affected by noise than in the case of greater basins. Hence, further analytical results are not yet available and we have to rely on some numerical results in this section to obtain a deeper insight into CF and MCF. Numerical results for CF and MCF are obtained by applying them to the well-investigated two-dimensional Hénon map, given by

$$\begin{pmatrix} x_{t+1} \\ y_{t+1} \end{pmatrix} = \boldsymbol{f}(x_t, y_t) = \begin{pmatrix} y_t + c - a x_t^2 \\ b x_t \end{pmatrix}, \tag{4.1}$$

where $a, b, c \in \mathbb{R}$ are parameters. For many values of a, b, and c the map exhibits chaotic behavior [18]. In this work, numerical results are performed with the parameter values $a = 1.2$, $b = 0.3$, and $c = 1$. Hence, the greatest Lyapunov exponent of the map is $\Lambda_1 \approx 0.42$. The Jacobian of Eq. (4.1),

$$\boldsymbol{J} = \begin{pmatrix} -2ax & 1 \\ b & 0 \end{pmatrix} \tag{4.2}$$

has to be determined to find any point $\boldsymbol{z}$ in Eq. (4.1) that satisfies the stability condition. The index t is disregarded because we are not yet interested in the dynamical behavior of a map, but rather points on the function graph. The eigenvalues of $\boldsymbol{J}$ are

$$\lambda_{1,2} = -ax \pm \sqrt{(a^2x^2 + b)} \tag{4.3}$$

and from Eq. (4.3) it is easy to determine $\max|\boldsymbol{\lambda}_{1,2}| < 1$. Inserting the parameter values gives $\max|\boldsymbol{\lambda}_{1,2}| < 1$ if $x \in B$ with $B = [-0.291\,67, 0.291\,67]$, as seen in Fig. 1. Hence, $\boldsymbol{z}' = (z(1) \ \ 0.3z(1))$ for any $z(1) \in B$. Recall that B and $B_{-\boldsymbol{k}}$ are subsets of the basin of attraction for CF and MCF, respectively; see Propositions III.3 and III.5. Any initial point in B or $B_{-\boldsymbol{k}}$ will converge to the corresponding fixed point.

Note that y_{t+1} and, as a consequence, y_* are predetermined by x_t since $y_{t+1} = bx_t$. From this it follows that $k(2)$ can be neglected for CF and MCF and is set at 0. From set B we can thus derive that a fixed point can be reached by applying CF or MCF if $k(1)$ varies in the interval $k(1) = [-1.1021, -0.693\,75]$. Furthermore, the function graph of the two-dimensional Hénon map can be represented in only two dimensions if y_t is interpreted as a predetermined constant. This makes it more comfortable to illustrate the methods graphically, because from the previous statements $f_x(x) = y_t + 1 - 1.2x^2$ is obtained for the uncontrolled map and

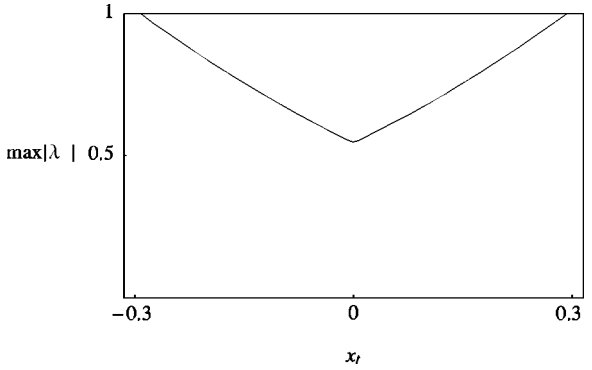

FIG. 1. Modulus of the greatest eigenvalue smaller than one obtained from Eq. (4.3) for the Hénon map ($a=1.2, b=0.3, c=1$).

$f_x^{CF}(x)=y_t+1-1.2x^2+k(1)$ is obtained for CF and $f_x^{MCF}(x)=y_t+1-1.2[x+k(1)]^2$ for MCF.

A. CF

Let $\boldsymbol{z}'=(0\ \ 0)$ with $|\lambda_{1,2}|=0.547\,72$ be the point to be shifted along the ordinate. Inserting $\boldsymbol{z}$ into Eq. (3.4) gives $\boldsymbol{k}'=(-1\ \ 0)$. Hence, Eq. (4.1) is modified to

$$\begin{pmatrix} x_{t+1} \\ y_{t+1} \end{pmatrix} = \begin{pmatrix} y_t+1-1.2x_t^2 \\ 0.3x_t \end{pmatrix} + \begin{pmatrix} -1 \\ 0 \end{pmatrix} \tag{4.4}$$

and the new map possesses an asymptotically stable fixed point at $\boldsymbol{x}'_*=\boldsymbol{z}'=(0\ \ 0)$, as can be seen in Fig. 2(a), with $y_t=y_*=0$. The graph of f_x, with $f_x(0)=1$, is shifted downwards along the ordinate until f_x intersects the 45° line at $\boldsymbol{z}$. A dynamical presentation of CF is given in the x_{t+1} vs x_t plot in Fig. 2(b). Starting from the initial conditions $x_0=0.5$ and $y_0=1$, the map converges to the fixed point. The iterates x_t lie on different graphs of f_x^{CF}, depending on y_t; for instance, the first graph is plotted from $f_x^{CF}(x)=y_0+1-1.2x^2+k(1)$ and the second from $f_x^{CF}(x)=y_1+1-1.2x^2+k(1)$.

Sometimes existing chaos has to be controlled, i.e., control can only be switched on after some finite iterations of the map. In Fig. 3 the successive iterates of the Hénon map

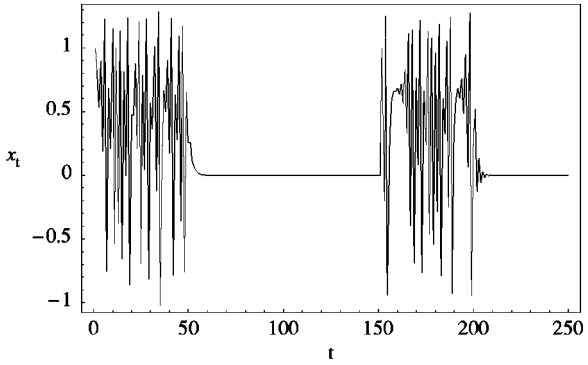

FIG. 3. Iterates x_t of the Hénon map ($a=1.2$, $b=0.3$, $c=1$) controlled by CF with $x_0=1, y_0=0.5$ and $k(1)=0$ for iteration $0\leqslant t\leqslant 50$, $k(1)=-1$ for $51\leqslant t\leqslant 150$, $k(1)=0$ for $151\leqslant t\leqslant 200$ and $k(1)=-1$ for $201\leqslant t\leqslant 250$.

subjected to CF after 50 and 200 iterations are depicted. In absence of CF from $0\leqslant t\leqslant 50$ and from $151\leqslant t\leqslant 200$, the map exhibits chaotic behavior. Nevertheless, applying CF can be critical because it is not possible to achieve from Theorem III.2 the whole basin of attraction that guarantees convergence to a stable fixed point. This depends on the individual function vector $\boldsymbol{f}$ and on the strength of $\boldsymbol{k}$. Therefore, a basin of attraction is provided for the controlled $\boldsymbol{k}'=(-1\ \ 0)$ and the uncontrolled $\boldsymbol{k}'=(0\ \ 0)$ case. A grid of 300×300 points from $-3\leqslant x_0\leqslant 3$ and $-3\leqslant y_0\leqslant 3$ served as initial conditions for the Hénon map to find out whether the controlled system converges to the fixed point or diverges and whether the uncontrolled system converges to the chaotic attractor or diverges.

The basin of attraction is depicted in Fig. 4, in which the white area denotes the diverging set of initial conditions of both systems; the gray area denotes the attracting set of the chaotic attractor and the diverging set of the fixed point; the black area denotes the attracting set of the chaotic attractor and of the fixed point. As shown, the basin of attraction shrinks if the map is subjected to CF. It is thus obvious that CF can only be activated to control a chaotic map if a trajectory starts in or enters the black area.

Now let us consider the effect of noise on CF. Hence, an independently identically distributed random variable ϵ_t

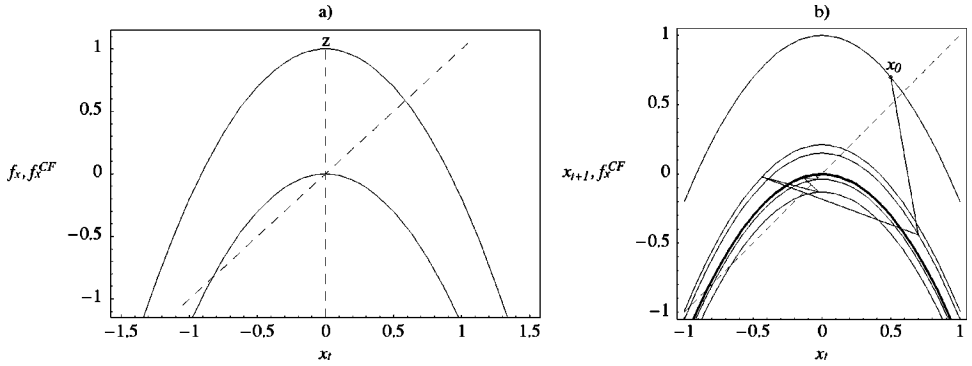

FIG. 2. (a) The point $\boldsymbol{z}'=(0\ \ 0)$ on the graph f_x of the Hénon map ($a=1.2$, $b=0.3$, $c=1$) is shifted with $\boldsymbol{k}'=(-1\ \ 0)$ such that the graph of f_x^{CF} intersects the 45° line at $\boldsymbol{z}$ and becomes an asymptotically stable fixed point. b) From the initial conditions $x_0=0.5$, $y_0=1$ and with $\boldsymbol{k}'=(-1\ 0)$ the Hénon map ($a=1.2$, $b=0.3$, $c=1$) converges to the fixed point $\boldsymbol{z}$. For each iteration $f_x^{CF}(x)=y_t+1-1.2x^2+k(1)$ is plotted.

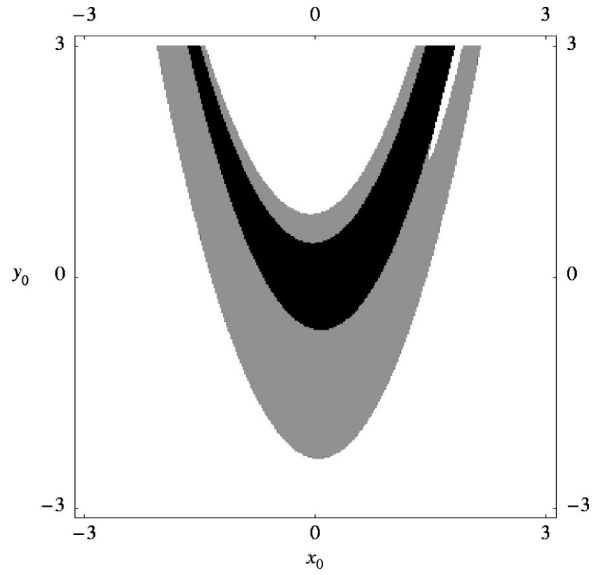

FIG. 4. Basin of attraction of the controlled [CF,$k'=(-10)$] and uncontrolled Hénon map ($a=1.2$, $b=0.3$, $c=1$). White area: diverging set for both maps. Gray area: attracting set of the chaotic attractor and diverging set of the fixed point. Black area: attracting set of the fixed point and of the chaotic attractor.

$\sim Normal(0,\sigma)$ is added to x_{t+1} at each time step while the map is controlled by CF. The feedback is increased in 100 equal steps from $-1.1021<k_1<-0.693\,75$, which is the interval that guarantees stable fixed points in a system without noise. The standard deviation varies in the interval $0\leqslant\sigma\leqslant 0.21$ with $\Delta\sigma=0.005$. For each σ, $k(1)$ combination a transient phase of 5000 values of x_t is simulated to ensure that a trajectory evolves near the fixed point attractor. Assuming that the process was ergodic, then another $m=5000$ values of x_t were used to compute $\Delta\hat{s}=\hat{s}-\sigma$ of trajectories starting at $x_0=y_0=0$, where $\hat{s}=\sqrt{1/(m)\Sigma_{i=1}^{m}(x_{t-i}-x_*)^2}$ is the estimated standard deviation. Recall that the environment around the fixed point is still nonlinear. Then $\Delta\hat{s}$ can be interpreted as additional fluctuation induced by the added random shocks. The result can be found in Fig. 5 as a contour plot. White denotes σ, $k(1)$ combinations forcing the map to diverge to infinity and darker gray levels denote higher $\Delta\hat{s}$ values, i.e., higher additional fluctuations. High values for $k(1)$ go along with higher additional fluctuations because of very long transient phases. In the interval $-1\leqslant k(1)\leqslant -0.9$ we have a short transient phase and thus less additional fluctuation, but the map tends to be unstable. The estimated standard deviation $\hat{s}\approx 0.68$ of the chaotic Hénon map without noise serves as a reference case. If white noise is added, the chaotic system tends to be unstable for $\sigma>0.04$. Note that CF cannot filter noise but is able to reduce the chaotic fluctuations, as can be seen in Fig. 5. Furthermore, if CF is applied the dynamical system becomes more robust against noise since random variables with a standard deviation five times higher than in the chaotic case can be added to the map.

Finally, we turn to accessing periodic orbits by applying CF. Therefore, the bifurcation diagram in Fig. 6(a) and the

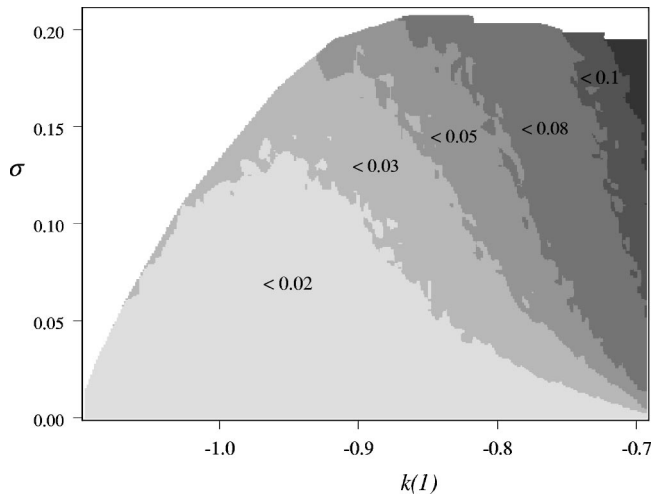

FIG. 5. Contour plot shows $\Delta\hat{s}=\hat{s}-\sigma$ for fixed points; initial conditions: $x_0=0$ and $y_0=0$.

Lyapunov spectrum in Fig. 6(b) are computed for the controlled Hénon map. The feedback parameter $k(1)$ is varied to produce different system dynamics. The map is unstable for $k(1)<-1.1021$ and has fixed points for $-1.1021<k(1)<-0.693\,75$. We can find a period doubling bifurcation at $k(1)=-0.693\,75$, where $\Lambda_1=0$. Thus, periodic orbits can be accessed for $k(1)>-0.693\,75$. The map returns to a chaotic phase for $k(1)>0.115$, which is interrupted by some stable higher periodic orbits. The map becomes unstable for parameter values $k(1)>0.187$. As we can see, it is possible to steer trajectories to different periodic orbits by simply varying the feedback parameter.

B. MCF

Applying MCF to Eq. (4.1) with $\boldsymbol{k}'=(k(1)\ \ k(2))$, the Hénon map is modified to

$$\begin{pmatrix} x_{t+1} \\ y_{t+1} \end{pmatrix} = \begin{pmatrix} [y_t+k(2)]+c-a[x_t+k(1)]^2 \\ b[x_t+k(1)] \end{pmatrix}. \qquad (4.5)$$

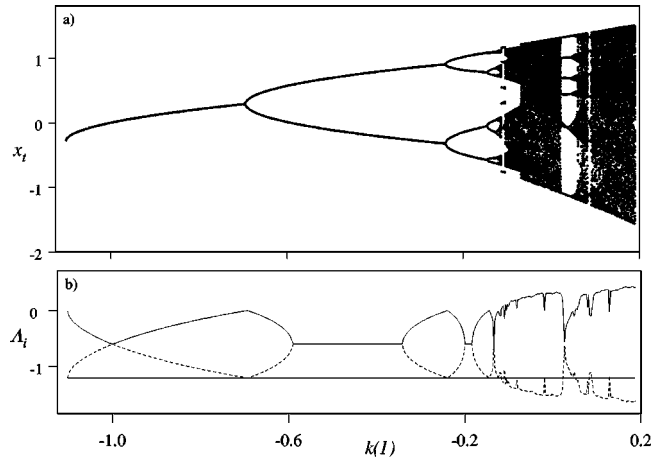

FIG. 6. (a) Bifurcation diagram and (b) Lyapunov spectrum for the Hénon map ($a=1.2$, $b=0.3$, $c=1$) subjected to CF with $x_0=1$ and $y_0=0.5$ and $k(1)=[-1.1021,0.187]$.

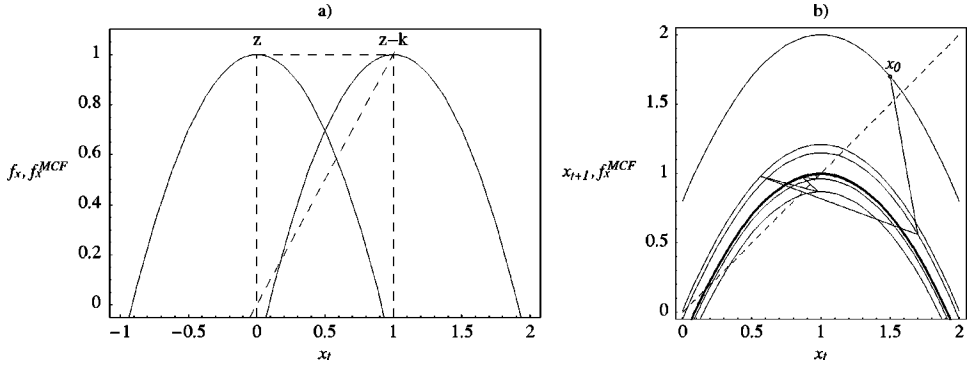

FIG. 7. (a) The point $\boldsymbol{z}'=(0\ 0)$ on the graph f_x of the Hénon map ($a=1.2$, $b=0.3$, $c=1$) is shifted with $\boldsymbol{k}'=(-1\ \ 0)$ such that the point $\boldsymbol{z}-\boldsymbol{k}$ on the graph f_x^{MCF} intersects the 45° line and becomes an asymptotically stable fixed point. (b) From the initial conditions $x_0=1.5$, $y_0=1$ and with $\boldsymbol{k}'=(-1\ \ 0)$ the Hénon map ($a=1.2$, $b=0.3$, $c=1$) converges to the fixed point $\boldsymbol{z}-\boldsymbol{k}$. For each iteration $f_x^{MCF}=y_t+1-1.2[x_t+k(1)]$ is plotted.

Let $\boldsymbol{z}'=(0\ \ 0)$ with $|\lambda_{1,2}|=0.547\,72$ be the point to be shifted along the ordinate. Inserting $\boldsymbol{z}$ in Eq. (3.7) gives $\boldsymbol{k}'=(-1\ \ 0)$. Hence, inserting the parameter values into Eq. (4.5) results in

$$\begin{pmatrix} x_{t+1} \\ y_{t+1} \end{pmatrix} = \begin{pmatrix} y_t + 1 - 1.2(x_t - 1)^2 \\ 0.3(x_t - 1) \end{pmatrix} \tag{4.6}$$

and the new map possesses an asymptotically stable fixed point at $\boldsymbol{x}'_*=\boldsymbol{z}'-\boldsymbol{k}'=(1\ \ 0)$, as seen in Fig. 7(a), with $y_t=y_*=0$. The graph of $f_x^{MCF}(x)$ is shifted to the right until it intersects the 45° line at $\boldsymbol{z}-\boldsymbol{k}$. Figure 7(b) represents a dynamical view on MCF with initial conditions $x_0=1.5$ and $y_0=1$. The iterates x_t converge to the fixed point and lie on different graphs of $f_x^{MCF}(x)$, depending on y_t; for instance, the first graph is plotted from $f_x^{MCF}(x)=y_0+1-1.2[x+k(1)]^2$.

In Fig. 8 an example is given to demonstrate the efficiency of MCF if the system already evolves on the chaotic attractor. Starting from the initial conditions $x_0=1$ and $y_0=0.5$, the Hénon map evolves 50 iterations on a chaotic attractor before the control method is activated. Then the map rapidly converges to the fixed point $\boldsymbol{x}'_*=\boldsymbol{z}'-\boldsymbol{k}'=(1\ \ 0)$. Setting MCF off after 150 iterations, the map reverts to chaotic behavior and after 200 iterations it converges to $\boldsymbol{z}'-\boldsymbol{k}'$, as it is again subjected to MCF.

The basin of attraction for the controlled and uncontrolled Hénon map is depicted in Fig. 9. It is obtained using the same procedure as in the case of CF. The white area denotes the diverging set of initial conditions of both systems; the light gray area denotes the attracting set of the chaotic attractor and the diverging area of the fixed point; the dark gray area denotes the attracting set of the fixed point and the diverging area of the chaotic attractor; the black area denotes the attracting set of the chaotic attractor and the fixed point attractor. The basin of attraction shrinks if MCF is applied and, in addition, it is also shifted to the right. It is thus obvious that MCF can only succeed in controlling the cha-

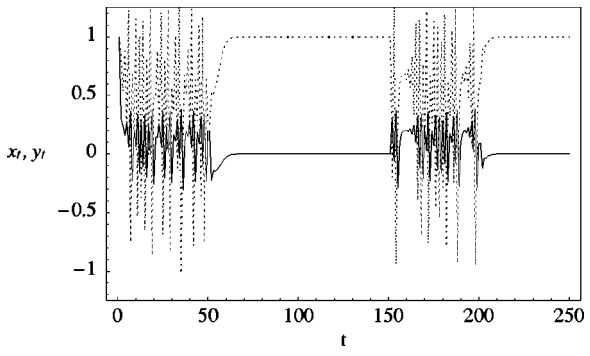

FIG. 8. Iterates x_t (dotted-line curve) and y_t (solid line curve) of the Hénon map ($a=1.2$, $b=0.3$, $c=1$) controlled by MCF with $x_0=1, y_0=0.5$ and $k(1)=0$ for iteration $0\leqslant t\leqslant 50$, $k(1)=-1$ for $51\leqslant t\leqslant 150$, $k(1)=0$ for $151\leqslant t\leqslant 200$, and $k(1)=-1$ for $201\leqslant t\leqslant 250$.

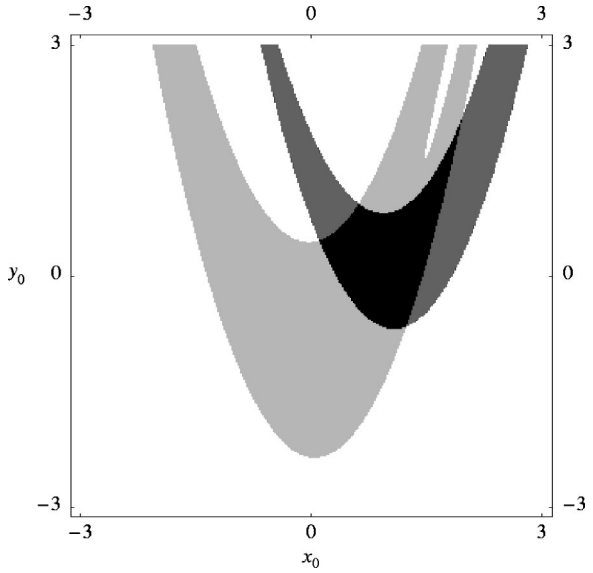

FIG. 9. Basin of attraction of the controlled [MCF,$\boldsymbol{k}'=(-10)$] and uncontrolled Hénon map ($a=1.2$, $b=0.3$, $c=1$). White area: maps diverge. Light gray area: attracting set of the chaotic attractor and diverging set for the fixed point. Dark gray area: attracting set of the fixed point and diverging set of the chaotic attractor. Black area: attracting set of the fixed point and of the chaotic attractor.

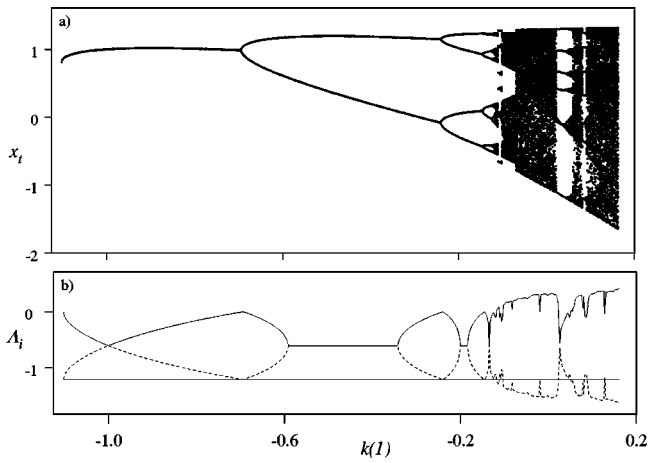

FIG. 10. (a) Bifurcation diagram and (b) Lyapunov spectrum of the Hénon map ($a=1.2$, $b=0.3$, $c=1$) subjected to MCF with $x_0=1$ and $y_0=0.5$ and $k(1)=[-1.1021,0.1622]$.

otic Hénon map if it is activated when a trajectory enters the black area.

The influence of noise on MCF is investigated in the same manner and with the same pseudorandom-numbers as in the case of CF. Different initial conditions $x_0=1$ and $y_0=0.5$ are used, but the results differ only marginally, i.e., almost the same values for $\Delta\hat{s}$ are obtained. This stems from the fact that the same points of the graph of the function vector are shifted as in the case of CF, possessing the same dynamical properties. The only difference is that the graph is now shifted along the abscissae. Consequently, MCF is also not able to filter noise, but is robust against noise and reduces the chaotic fluctuations.

Finally, we turn to accessing periodic orbits by applying MCF. Therefore, the bifurcation diagram in Fig. 10(a) and the Lyapunov spectrum in Fig. 10(b) are computed for the controlled Hénon map. The feedback parameter $k(1)$ is varied to produce different system dynamics. The map is unstable for $k(1)<-1.1021$ and has fixed points for $-1.1021<k(1)<-0.693\,75$. We can find a period doubling bifurcation at $k(1)=-0.693\,75$, where $\Lambda_1=0$. Thus, periodic orbits can be accessed for $k(1)>-0.693\,75$. The map returns to a chaotic phase at $k(1)\approx 0.115$, which is interrupted by some stable higher periodic orbits. The map becomes unstable for parameter values $k(1)>0.187$. As we can see, it is possible to steer trajectories to different periodic orbits by simply varying the feedback parameter. Note that the identical Lyapunov spectrum is obtained as in the case of CF. Only one difference arises, since applying MCF yields a system breakdown for $k(1)>0.1622$ instead of $k(1)>0.187$ for CF. Furthermore, the bifurcation diagram in Fig. 10(a) is only shifted in the phase space by the amount of $k(1)$ if it is compared with the bifurcation diagram for CF.

C. Determining the constant feedback vector from time series

In the preceding section the calculation of the constant feedback vector **k** is based on the *a priori* knowledge of the map, which in most practical cases is unrealistic. There are two ways to solve this dilemma. First, if the dimension of the system is known each element $k(i)$, $i=1,\ldots,n$ of **k** could be successively increased or decreased. Unfortunately, this gives 2^n possible combinations to proceed, starting from $\mathbf{k}=0$, and is thus inapplicable for higher dimensions. A much better way is to determine **k** from time series information. This is done in this section with the help of a simple algorithm, which may be slow due to computing time but illustrates the theoretical context. Conceptually, the algorithm structures as follows: (1) sort the time series to find nearest-neighbor points, (2) approximate the maximum eigenvalue, and (3) calculate **k** from nearest-neighbor points.

(1) Consider a time series $(\mathbf{x}_1,\mathbf{x}_2,\ldots,\mathbf{x}_t)$ with $\mathbf{x}_i\in\mathbb{R}^n$. The first step is to form pairs $\{\mathbf{x}_i,\mathbf{x}_j\}$, where an $\mathbf{x}_j$ is assigned to an $\mathbf{x}_i$ if the condition

$$\min\|\mathbf{x}_i-\mathbf{x}_j\|<\omega \quad \forall j\neq i \tag{4.7}$$

is satisfied. Here $\|\cdot\|$ denotes the Euclidean norm and ω is a suitable radius of a ball around $\mathbf{x}_i$. Thus, a pair $\{\mathbf{x}_i,\mathbf{x}_j\}$ contains nearest neighbors with a distance smaller than ω.

(2) Starting from $\mathbf{x}_i$ and $\mathbf{x}_j$, respectively, we can observe the next iterations $\mathbf{x}_{i+1}$ and $\mathbf{x}_{j+1}$ and approximate the greatest eigenvalue at $\mathbf{x}_i$ with

$$\lim_{\omega\to 0}\frac{\|\mathbf{x}_{j+1}-\mathbf{x}_{i+1}\|}{\|\mathbf{x}_j-\mathbf{x}_i\|}\approx\lambda_{max_i}. \tag{4.8}$$

This approach is used, for example, in the Wolf algorithm to calculate the greatest Lyapunov exponent from time series [19].

(3) If $|\lambda_{max_i}|<1$, then $\mathbf{x}_i$ is a possible new fixed point. Thus, from Eq. (3.7) and Eq. (3.4) the constant feedback vector can be determined by $\mathbf{k}=\mathbf{x}_i-\mathbf{f}(\mathbf{x}_i)$, where $\mathbf{f}(\mathbf{x}_i)=\mathbf{x}_{i+1}$, and it follows that

$$\mathbf{k}=\mathbf{x}_i-\mathbf{x}_{i+1}. \tag{4.9}$$

This algorithm is obviously vague for a great radius ω or in the presence of noise. In this case a set $\{\mathbf{x}_t\}$ of several nearby points can be used to estimate the eigenvalue by least squares, as, for example, in Ref. [20]. Additionally, we have to estimate the real successor $\mathbf{x}_{t+1}$.

Note that we do not use a time series reconstructed from a one-dimensional time series by a time-delay method [21]. Although first numerical results show that the maximal eigenvalue can be approximated well, it is not yet possible to calculate **k** from this kind of data.

V. CONCLUSION

With CF and MCF, simple methods for controlling chaos in higher-dimensional discrete maps have been introduced. It was shown analytically that chaotic attractors can be converted to fixed point attractors if a constant feedback vector is added to the system function (CF) or if the input vector is superimposed by a constant feedback vector (MCF). The basic idea in both methods is to shift the graph of the function vector of a map. A method to choose an appropriate constant

feedback vector for controlling chaotic systems is achieved from Theorems III.2 or III.4. It is obvious, because of the weak requirements referring to the function vector $\boldsymbol{f}$ of a map, that CF and MCF guarantee chaos control for almost every map, e.g., high-dimensional coupled map lattices. Unfortunately, this good news makes it difficult to find a basin of attraction for initial conditions such that a map is attracted to the fixed point. Therefore, rigorous conditions for system function vectors have to be set up, as Gueron illustrated for the one-dimensional case [9]. However, as it is known that $\boldsymbol{z}$ in Theorem III.2 and $\boldsymbol{z}-\boldsymbol{k}$ in Theorem III.4 represent asymptotic stable fixed points, it is guaranteed that there exist at least small neighborhoods of initial conditions converging to $\boldsymbol{z}$ and $\boldsymbol{z}-\boldsymbol{k}$, respectively. An extension of this idea was formalized in Propositions III.3 and III.5. Numerical examples were given as CF and MCF were applied to the Hénon map; it was also shown that periodic states are accessible.

Besides their simple implementation, since we do not have to collect data for the computation of parameter perturbations or feedbacks, both CF and MCF methods possess further advantages with regard to the other methods. Since no updated information on the state of the system is required, no latency due to measuring and computing control signals is wasted and thus chaos control in the GHz range is imaginable. Furthermore, by applying CF or MCF, the dimensionality of a system does not increase, unlike with the DFC method, because $\boldsymbol{k}$ is a constant. Due to robustness against noise, CF and MCF are superior to OGY since the use of linear approximation in small vicinities of certain points is renounced. These methods do not change system parameters, which may be fixed by the properties of the investigated map. Additionally, note that CF and MCF can be applied to nonchaotic maps, e.g., maps converging to a stable fixed point can be steered to other fixed points or chaotic regions if desired. As for OGY, targeting and DFC, the application of CF and MCF does not imply *a priori* knowledge of the system equations, since control can be achieved by successively ascending or descending the constant feedback parameter. In addition, it has been shown for the first time of CF and MCF that possible new fixed points as well as the constant feedback vector can be determined from time series information. Finally, the application of CF and MCF is not limited by certain characteristics of a map, like finite torsion in the case of DFC, or relatively small Lyapunov exponents compared to the discrete time steps, as in the case of OGY.

[1] F.J. Dyson, *Infinite in All Directions* (Harper and Row, New York, 1988).

[2] E. Ott, C. Grebogi, and J.A. Yorke, Phys. Rev. Lett. **64**, 1196 (1990).

[3] K. Pyragas, Phys. Lett. A **170**, 421 (1992).

[4] B. Huberman and E. Lumer, IEEE Trans. Circuits Syst. **37**, 547 (1990).

[5] S. Sinha, R. Ramaswamy, and J. Rao, Physica D **43**, 118 (1990).

[6] L. Molgedey, J. Schuchhardt, and H.G. Schuster, Phys. Rev. Lett. **69**, 3717 (1992).

[7] S. Rajasekar and M. Lakshmanan, Physica D **67**, 282 (1993).

[8] S. Parthasarathy and S. Sinha, Phys. Rev. E **51**, 6239 (1995).

[9] S. Gueron, Phys. Rev. E **57**, 3645 (1998).

[10] N. Parekh, S. Parthasarathy, and S. Sinha, Phys. Rev. Lett. **81**, 1401 (1998).

[11] N. Parekh and S. Sinha, Santa Fe Institute report, 2000 (unpublished).

[12] G. Osipov, L. Glatz, and H. Troger, Chaos, Solitons Fractals **9**, 307 (1998).

[13] N.J. Corron, S.D. Pethel, and B.A. Hopper, Phys. Rev. Lett. **84**, 3835 (2000).

[14] C. Wagner and R. Stoop, Phys. Rev. E **63**, 017201 (2001).

[15] E. Korpimäki and K. Norrdahl, Ecology **79**, 2448 (1998).

[16] P. Hudson, A. Dobson, and D. Newborn, Science **282**, 2256 (1998).

[17] S. Wiggins, *Introduction to Applied Nonlinear Dynamical Systems and Chaos* (Springer, Berlin, 1990).

[18] M. Hénon, Commun. Math. Phys. **50**, 69 (1976).

[19] A. Wolf, J.B. Swift, H.L. Swinney, and J.A. Vastano, Physica D **16**, 285 (1985).

[20] J.-P. Eckmann, S.O. Kamphorst, D. Ruelle, and S. Ciliberto, Phys. Rev. A **34**, 4971 (1986).

[21] N. Packard, J. Crutchfield, D. Farmer, and R. Shaw, Phys. Rev. Lett. **45**, 712 (1980).